Proton nuclear magnetic resonance J-spectroscopy of phantoms containing brain metabolites on a portable 0.05 T MRI scanner

Ronen, I.; O'Reilly, T.; Froeling, M.; Webb, A.G.

Journal of Magnetic Resonance 320 (2020) 106834

Contents lists available at ScienceDirect

Journal of Magnetic Resonance

journal homepage: www.elsevier.com/locate/jmr

Proton nuclear magnetic resonance J-spectroscopy of phantoms containing brain metabolites on a portable 0.05 T MRI scanner

Itamar Ronen [a,*], Thomas O'Reilly [a], Martijn Froeling [b], Andrew G. Webb [a]

[a] C. J. Gorter Center for High Field MRI, Department of Radiology, Leiden University Medical Center, Leiden, the Netherlands
[b] Department of Radiology, University Medical Center Utrecht, Utrecht, the Netherlands

ARTICLE INFO

Article history:
Received 8 June 2020
Revised 19 September 2020
Accepted 21 September 2020
Available online 24 September 2020

Keywords:
Low field MRI
Magnetic Resonance Spectroscopy
J-spectroscopy
Brain metabolites

ABSTRACT

We examined approaches for obtaining ^{1}H NMR spectra of brain metabolites on a low-field (B_0 = 0.05 T) portable MRI scanner, which was developed in our laboratory with the aim of bringing cost-effective radiological services to populations in underserved, remote regions. The low static magnetic field B_0 dictates low signal to noise ratio for metabolites in the mM concentration range, and results in an overall spectral region for the ^{1}H resonances of these metabolites narrower than the linewidth obtainable in our scanner. The narrow spectral range also precludes the possibility of suppressing the large contribution of the water resonance at the acquisition stage.

We used a spectroscopic Carr-Purcell-Meiboom-Gill (CPMG) sequence to acquire multiecho data from solutions of J-coupled brain metabolites, focusing on lactic acid, a metabolite whose concentration is negligible in the healthy brain and increases significantly in several disease conditions. The J spectra we obtained for lactate from the Fourier transformation of the multiecho data are spectrally well-resolved for a range of echo spacing values. We show that the J spectra at different echo spacings fit well with simulations of the evolution of echo train signal of the lactate under the same conditions. Applying a J-refocused variant of the CPMG sequence, the J modulation of the echo decay is removed, providing a way for subtracting the large contribution of the non-modulated component in the J spectrum in conditions where notching it using post-processing methods is impossible. We also demonstrate by means of experimental data and simulations that in our experimental conditions, J-spectra of other prominent brain metabolites, such as the neurotransmitter glutamate, do not yield discernible peaks and only contribute to a broad peak at zero frequency.

1. Introduction

Recently there has been a growing interest in low field MRI (<0.1 Tesla) for potential medical applications [1–4]. Significant improvements in magnet design, RF and gradient hardware and post-processing technologies make it possible to use such systems to generate good quality low field MRI data of the human brain and other anatomies [5–10]. This, coupled with the relatively low cost and portability of such systems make them ideal for distribution in areas of the world in which medical imaging is scarce or non-existent, and where simple, targeted solutions addressed by low field MRI can make a significant difference in health care outcome.

While the main focus is on imaging applications of low field systems, medical applications of ^{1}H NMR spectroscopy can be also envisioned. Several devastating brain diseases are marked by drastic change, either local or global, in the concentrations of metabolites which are detectable by ^{1}H NMR spectroscopy [11]. For example, in neonatal ischemic hypoxia caused by insufficient oxygen delivery to the brain at birth, ^{1}H NMR spectroscopy shows a significant global increase in lactate concentration, and its presence in the NMR spectrum is considered to be the most reliable marker for the pathology, as well as the one most correlated with the clinical outcome [12,13].

In-vivo applications of ^{1}H NMR spectroscopy using MRI scanners operating at low field come with significant challenges. First and foremost is the low signal to noise ratio (SNR), dictated both by the well-known relationship between the strength of the static magnetic field B_0 and the resulting NMR signal, as well as by the low concentration of the molecules of interest. Brain metabolites prominent in the ^{1}H NMR spectrum, such as N-acetyl aspartate (NAA), glutamate (Glu), creatine compounds (tCr), choline compounds (tCho) and myo-inositol (Ins) are in the mM concentration

* Corresponding author at: LUMC/Radiology C3Q, Albinusdreef 2, Leiden 2333ZH, The Netherlands.
E-mail address: i.ronen@lumc.nl (I. Ronen).

https://doi.org/10.1016/j.jmr.2020.106834
1090-7807/

range, 3–4 orders of magnitude less than water protons. For example, lactate, a marker for a host of brain disorders, including metabolic disorders, tumors, stroke and hypoxic ischemia increases from negligible concentrations to about 10 mM in affected areas in the diseased brain [11]. Added to the SNR challenge is also the small chemical shift separation at low field of the spectral contribution of these metabolites. The spectral range of most of the ^{1}H resonances of biologically-relevant molecules is about 3 ppm, corresponding to about 6 Hz at B_0 = 0.05 T. This has several ramifications: one is that ^{1}H NMR spectra obtained using simple pulse sequences are extremely susceptible to any factor that affects the spectral linewidth, most significantly B_0 inhomogeneity intrinsic to the magnet design. Because of the low SNR at low-field, spectroscopic experiments are performed on large volumes, and typically without any spectral localization. In such conditions the effectiveness of B_0 shimming is very limited. As a result, typical linewidth over the measured volume in such experiments is larger, and sometimes significantly so, than the entire span of resonances of interest. Secondly, at B_0 = 0.05 T, $\delta \approx J$ for practically all molecules of interest, where δ is a typical chemical shift difference between resonances in a molecule, J the proton-proton scalar coupling constant (typically about 4–8 Hz for vicinal protons and about −12 Hz for geminal protons). The proton spectra of all metabolites are then strongly coupled, not only complicating the spectra of even simple molecules, but also resulting in weak outer spectral lines. An example is given in Fig. 1, where simulated spectra of the lactate ion ($CH_3CH(OH)COO^-$) at 7 T and 0.05 T are shown. The scalar coupling constant J between the CH_3 and the CH protons is 6.9 Hz and the chemical shift difference between the CH_3 and the CH protons is 2.8 ppm [14], which is equivalent to 836 Hz at 7 T and to 6 Hz at 0.05 T. At 7 T the lactate spectrum is that of an AX_3 system and comprises the readily recognizable 1:1 doublet of the CH_3 group and the 1:3:3:1 quartet of the CH proton. At 0.05 T the lactate spectrum becomes that of a AB_3 system. The spectrum of an AB_3 system has been fully explained in a work by Diehl et al.[15]. Briefly, the transitions that give rise to the spectrum can be assigned to contributions from two spin systems: an AB system in which I_A = ½ and I_B = ½ and an AB system in which I_A = ½ and I_B = 3/2, where I_A is the total spin number of the CH proton and I_B is the total spin number of the CH_3 proton group. The contribution of the [I_A = ½ I_B = ½] AB systems is marked with arrows. The frequency difference between the two outer spectral lines of the AB sub-spectrum, covering most of the overall spectral content of the AB_3 spectrum, is given by: $J + \sqrt{J^2 + \delta^2}$ (see for example [16], p. 50). In the case of lactate at 0.05 T, this translates to a frequency range of 16 Hz.

Another significant challenge resulting from the narrow spectral range concerns the removal of the water peak from the spectrum. Water suppression via chemical shift selection/suppression in the acquisition stage relies solely on the spectral separability of the water resonance from other peaks in the spectrum, and this becomes impossible to perform when the spectral range is equal or even smaller than the water line width.

Rather than using sequences which are variations on pulse-acquire, the use of data collected as a series of spin-echoes provides a solution for some of the challenges stated above. While

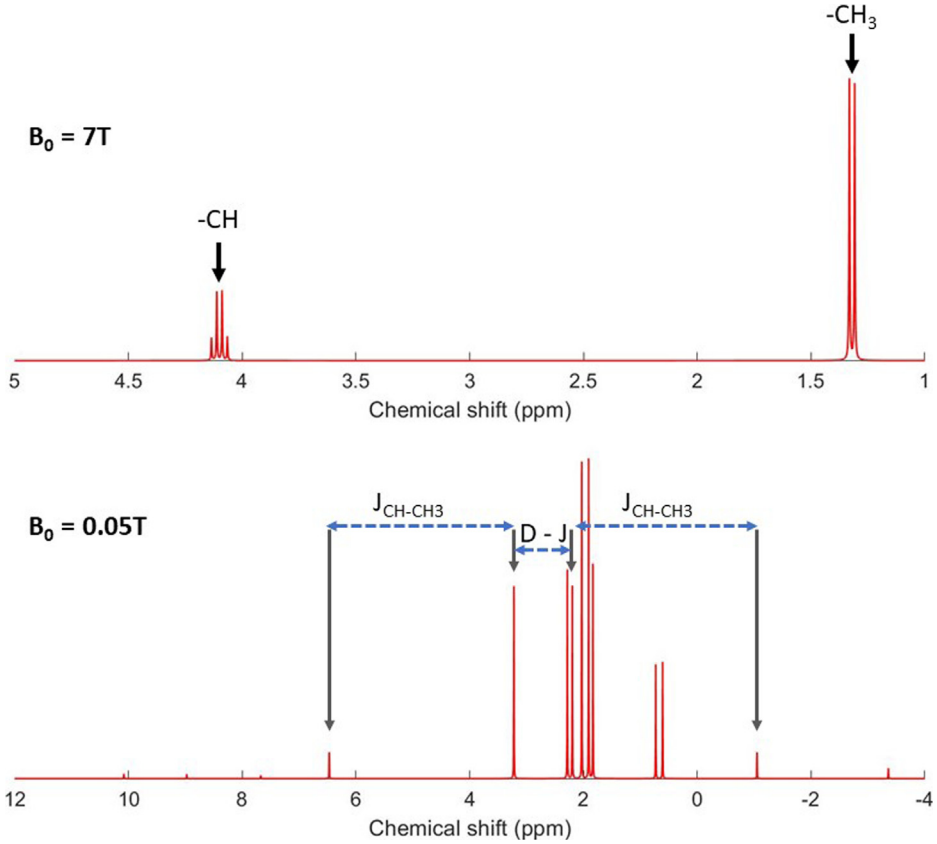

Fig. 1. Simulations of the NMR spectrum of lactate at two different static magnetic fields. Top: B_0 = 7 T; Bottom: B_0 = 0.05 T, the field in which all experiments in this work have been performed. Line width of 2 Hz (top) and 0.001 Hz (bottom) was added for visual purposes. The spectrum at 7 T shows the well separated CH_3 doublet and CH quartet, each showing the 7 Hz splitting generated by the scalar coupling between the two proton groups. The spectrum at 0.05 T is the superposition of two AB sub-spectra: one in which [I_{CH} = 1/2 , I_{CH3} = 1/2] and one in which [I_{CH} = ½ , I_{CH3} = 3/2]. The contribution of the first sub-spectrum is marked by gray arrows. The frequency spacings and amplitude ratios are according to the standard expressions given for AB spectra: the outer lines are separated by J (6.95 Hz in this case) and the inner lines are separated by D – J, where $D = \sqrt{J^2 + \delta^2}$, where δ is the chemical shift difference between the CH and the CH_3 resonances. At 0.05 T, δ = 6 Hz.

the chemical shift, together with all B_0-dependent frequency variations, are refocused by a 180° pulse, homonuclear spin–spin coupling continues to evolve [17–19]. Thus, a series of echoes acquired sequentially or with a single excitation with a spectroscopic Carr-Purcell-Meiboom-Gill (CPMG) sequence [20] contains the spectral information of the standard FID in each echo, while the signal along the echo train will evolve according to the underlying scalar couplings, providing the basis for the technique known as 2D J-resolved spectroscopy [21–23]. One particularly attractive property of the evolution of the echo series along the echo time dimension is that its decay rate is dictated by T_2 rather than T_2^*, and thus the linewidth along the ω_1 dimension in a 2D J-resolved experiment is much narrower and close to $1/\pi T_2$. This provides an opportunity for obtaining partial spectral information from spectroscopic CPMG sequences on J-coupled systems at low-field, even when the B_0 inhomogeneity masks all spectral information in the regular spectrum. The potential of J-resolved spectroscopy to provide separable spectral information on J-coupled metabolites has been suggested as a means to improve the detection of metabolites such as γ-amino butyric acid (GABA) in in-vivo NMR [24], and an imaging sequence based on spatial encoding of the J-modulated signal in a CPMG sequence has been suggested as a potential application at low field [25]. When $\tau \gg 1/J$, τ being the half the 180°-180° delay time in a CPMG experiment, the echo signal modulation does not depend on τ [17,26]. As τ becomes shorter, the echo modulation becomes more complex, especially in strongly couple systems, where beyond the AB case [17] there is no available analytical solution: in this latter case it is possible to simulate of the time evolution of the spin system under CPMG using the density matrix formalism.

In this work we examined approaches for the acquisition of spectroscopic data at low field (B_0 = 0.05 T) from solutions of brain metabolites, with the purpose of examining the feasibility of obtaining such data *in-vivo* in a future setting. J spectra of two brain metabolites, lactate and glutamate, were acquired using a CPMG sequence with a variety of inter-pulse delays and compared to simulation results. Approaches for eliminating the contribution of water and other singlets to the central line of the J spectrum were tested. Finally, to provide a very preliminary evaluation of the ultimate feasibility of applying the method presented here to detect lactate *in-vivo* in disease conditions, we extrapolated data from a small sample of 100 mM concentration to estimate the expected SNR for a J spectrum of lactate at a concentration of 10 mM evenly distributed throughout the entire human brain with some improvements in the receive hardware and electronics.

2. Materials and methods

Hardware: All experiments were performed on a custom-built MRI scanner operating at B_0 = 0.05 T with a 27 cm diameter bore, described in detail previously [27] and shown in Fig. 2. The B_0 field is generated using a large number of permanent magnets arranged in a cylindrical dipolar Halbach array configuration and is directed across the bore of the scanner. Homogeneity over a 20 cm diameter spherical volume at the center of the magnet is 2400 ppm. Three linear gradient coils were constructed using an adapted target field method and are used to perform first order B_0 shimming over the sample [28]. A 3.5 cm diameter, 7 cm long solenoid wound with copper wire on a poly(methyl methacrylate) cylinder was used for as an RF transceiver coil. A spectrometer (Magritek Kea2, Aachen, Germany) was used to generate the low power RF pulses which were subsequently amplified by a custom built 1 kW RF amplifier [6,27]. The spectrometer features a built-in T/R switch used to route the amplified signal to the RF coil. The magnet is placed in a 62.5 × 62.5 × 85 cm Faraday cage constructed from aluminium sheets and extrusion profiles. An additional 50 μm thick copper sheet is used to line the bore of the magnet to shield the RF coil from any electromagnetic interference (EMI) coupled in to the system through the gradient coils. EM coupling can occur between the gradient coils and the RF coil in MR systems and thus can couple high frequency noise generated by the gradient amplifier directly in to the RF coil, negatively influencing the SNR. At low field the self-resonant modes of the gradient coils are close to the Larmor frequency and to the resonant frequency of the RF coil. When the RF coil is inserted into the scanner, the strong coupling of the self-resonant modes of the gradient to the RF coil causes detuning of the RF coil. A 50 μm thick copper sheet placed against the bore of the magnet, between the RF coil and the gradient coils reduces the impact of both of these interactions and is standard practice on high field systems.

Samples: solutions of lithium lactate and L-glutamic acid (>99%, Sigma Aldrich, St. Louis MO, USA) in D_2O (Sigma Aldrich, St. Louis MO, USA) and in H_2O were prepared. Both compounds were dissolved in tap water and in D_2O for samples with final concentration of 2 M. A 100 mM solution of lithium lactate in D_2O was also prepared. About 30 cc of each solution were subsequently injected into table-tennis balls, and the hole in the injection site was sealed with hot glue.

Pulse sequences: The sequences used for all experiments are shown in Fig. 3. The original CPMG sequence provided by the spectrometer manufacturer was modified to allow setting of the first echo time ($2\tau_1$) to be independent of subsequent echo times (2τ). This was done to minimize the phase accrual between the excitation pulse and the first echo. The CPMG sequence was also modified to generate the J-refocussed CPMG variant, where 90° pulses placed to coincide with the timing of even echo formation refocus the J evolution without affecting the evolution of the chemical shift [29]. In this sequence, data are acquired every other echo. The sequence is based on the "perfect echo" spin echo sequence, first suggested by Takegoshi et al.[30] and van Zijl et al.[31].

Experimental procedures: The phantom was positioned in the center of the RF coil, which was then placed in the center of the magnet, corresponding to the region of highest B_0 homogeneity. In all our experiments, no B_0 shimming was performed as the gradient amplifier introduced additional noise to the measurements. An initial pulse-and-collect sequence was used to automatically determine the resonance frequency. Subsequently, manual calibration of the RF power required for the 90° and 180° pulses was performed via acquisition of a series of spectra with varying RF power. A pulse length of 100 μs was used for 90° and 180° pulses in all experiments. Typical parameters for the CPMG acquisition were: TR = 20 s,: number of averages: 8 for the 2 M solutions and 32 for the 100 mM solution, bandwidth: 5 kHz, number of complex data points: 64 for an acquisition time of 12.8 ms symmetrically positioned around the echo time, initial echo time ($2\tau_1$ in Fig. 3): 16 ms, and a variety of inter-pulse delays (2τ) in the range of 50–125 ms. The number of echoes was either 128 or 256, with fewer echoes for the longer inter-pulse delays. The J-refocused CPMG sequence was applied to the same phantoms with identical acquisition parameters. Total acquisition time for the experiments with 8 averages (2 M solutions) was 2.5 min, and that of the experiments with 32 averages (100 mM solution) was 10 min.

Processing of multi-echo NMR data: complex data were exported from the spectrometer as CSV spreadsheet files. Each data set comprised an $N \times M$ matrix, N = number of points acquired at each echo, M = number of echoes. An additional ascii file contained salient acquisition parameters. These were read into Matlab® (Mathworks, Natick MA, USA) and analysed with in-house routines. Briefly: echo data from both sides of the echo peak were combined according to $S = S^+ + \mathrm{conj}(S^-)$, where S^+ comprises the data points

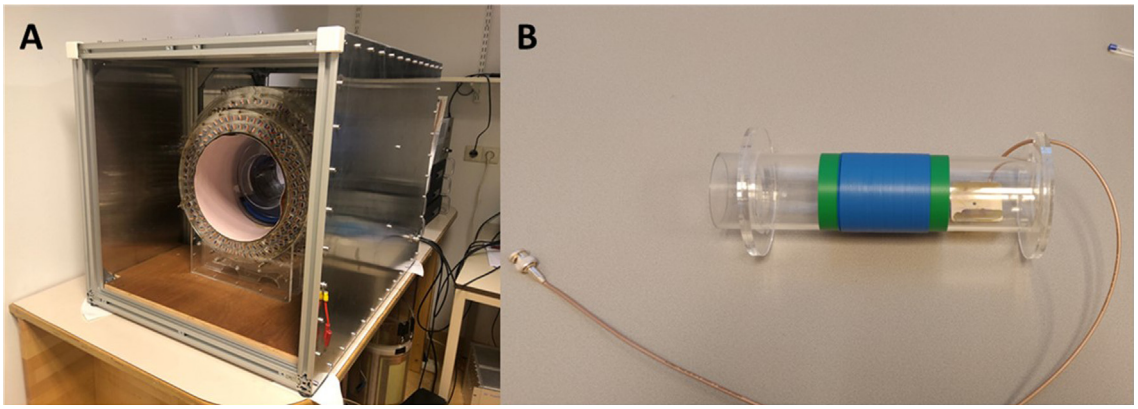

Fig. 2. (a) the NMR scanner on which experiments were performed; (b) the RF coil used. The coil was a solenoid with inner diameter = 3.5 cm.

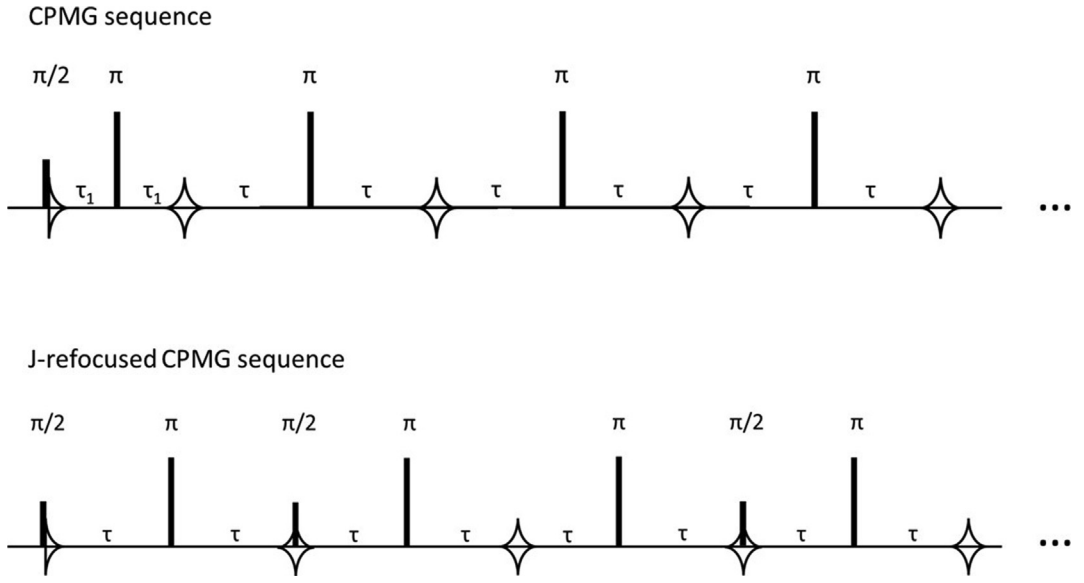

Fig. 3. Pulse sequences used in the NMR experiments. Top: standard CPMG sequence with tunable first delay; Bottom: J-refocused CPMG. In the latter, every second echo is acquired.

where $N/2 + 1 \leq n \leq N$, and S^- are the points where $1 \leq n \leq N/2$ in reverse order. Conj(S^-) represents the complex conjugate of S^-. The resulting "symmetrized" time-domain echo data was then Fourier transformed along the time domain to yield M complex spectra. The echo maximum was then used to yield a single complex value for each echo. The series of M echo maxima was zero-filled to 2*M and subsequently underwent Fourier transformation to yield the J-spectrum. For the phantoms with 2 M metabolite concentration no additional filtering/windowing was performed. Data obtained from the 100 mM solution of lactate was apodized with a damped exponential function matched with the linewidth of the main satellite peak in the J-spectrum, which was estimated at 0.13 Hz, using a Matlab code for spectral decomposition based on the Hankel singular value decomposition method (HSVD), see below for detailed description.

Spectral analysis: to obtain estimates on peak amplitudes and linewidth, as well as for subtracting specific peaks from the spectra, we used an in-house tool for spectral decomposition based on the Hankel singular value decomposition method (HSVD)[32]. The input for the HSVD routine was the complex time domain data (the J-spectrum data prior to the Fourier transformation), and input parameters included (1) the number of data points used for the autoregression part of the HSVD that provides the estimate for the frequencies and linewidths of the spectral components, typically ½ or ¼ of the total number of data points; (2) the bandwidth, dictated by the sampling rate, which in this case is equal to $1/(n\tau)$, where τ is half the inter-pulse delay of the CPMG sequence, n = 2 for the standard CPMG sequence and n = 4 for the J-refocused CPMG sequence; (3) the estimated rank (number of spectral components expected in the time series). A rank of 10–15 was sufficient to properly fit all spectra presented here, as well as to properly characterize the central peak for the subsequence subtraction of the water and singlet contribution (details are given in the relevant results chapter). The HSVD routine was also used to eliminate the narrow peak in the center of the J-spectrum, representing the contribution of non J-coupled spins, such as HDO and H_2O protons, to the J-spectrum. In that case, the HSVD routine was used with similar parameters to those used for the spectral fitting, and the narrow contribution to the center peak was empirically defined as any spectral component with linewidth smaller than 0.3 Hz and a frequency with an absolute value lower than 0.3 Hz, typically resulting in one or two spectral components, from which a synthetic time-domain signal was generated based on their amplitudes, frequencies, linewidths and phases, and subsequently subtracted from the original time domain data.

Simulations: All simulations were done with in-house Matlab® programs. For simulating the J-spectroscopy experiments, the signal $S^+(2n\tau)$ at the top of the n^{th} echo of a CPMG sequence with a π-π inter-pulse delay of 2τ was evaluated using the density matrix formalism, assuming a Hamiltonian that consisted of Zeeman and scalar coupling terms. RF pulses were assumed to be infinitely narrow pulses with initial nominal flip angles of $\pi/2$ and π [33,34] (for the Matlab-based simulation platform, see [35]). Deviations from the nominal flip angles, either because of inaccuracy in the flip angle determination or as a result of transmit radiofrequency field (B_1^+) inhomogeneity, result in mismatch between the experimental spectra and the simulation results. To partially account for this mismatch, simulations were performed with small variations in the flip angle, achieved by an scaling factor identically applied to the flip angle of both pulses. The scaling factor was between 0.9 and 1. Values for the chemical shifts and the scalar coupling values for lactate were taken from Govindaraju et al [14]. To provide a matching line width to the experimentally acquired J-spectra, simulated echo trains were multiplied with an exponential decay function that approximated the T_2 of the sample, prior to Fourier transform. Since simulation results may depend on the accuracy in setting the flip angles of the CPMG sequence, we simulated also the expected B_1^+ distribution generated by the solenoid coil across the phantom using the Biot-Savart equation. We provide the results of the B_1^+ simulation as supplementary material S1, where we also provide simulations lactate J-spectra generated with scaled-down flip angles, showing the potential effect of inaccurate flip angles on the resulting J-spectra.

3. Results

Fig. 4 shows a typical spectrum obtained from an FID collected from the 2 M Lac/H_2O phantom. For this and all other experiments reported here, no B_0 shimming was performed, and the resulting full width at half maximum (FWHM) of the single spectral line discernible in the spectrum was about 500 Hz. Fig. 5 shows data acquired with the standard CPMG sequence from phantom that contained 2 M lactate solution in D_2O. Panels a and b show typical multi-echo data acquired from this phantom, in this case with echo spacing of 83.3 ms. In this case, 256 echoes were acquired, with 64 samplings along each echo. In (a) the data are shown in the time domain, and in (b) in the frequency domain, following symmetrisation around the echo peak, zero-filling once and Fourier transformation. The amplitude modulation of the echo peaks caused by the scalar coupling is visible in both panels. Panel c shows time domain echo data acquired with three different inter-pulse delays, including the one of the data shown in panels a and b. The J modulation on the echo train in all three cases is clearly visible, and the J-spectra are generated by a Fourier transformation applied to these echo trains. The remaining panels d through h show the J-spectra obtained from similarly acquired data at 5 different inter-pulse delay values. These are shown along with simulated J-spectra for the same inter-pulse delay. The narrow contribution of uncoupled spins to the zero frequency component, predominantly corresponding to the fast exchanging —OH protons, was removed with a Matlab® Hankel singular value decomposition (HSVD) routine [32], as described in the methods section. Examples of J-spectra before and after subtraction of the narrow contribution to the center peak are provided for three values of inter-pulse delays in supplementary figure S2. The spectral features of the J-spectra vary significantly across inter-pulse delay values. The main spectral features of the experimental J-spectra are well represented in the simulation results, with some deviations, mostly at frequencies lower than 1 Hz and at longer inter-pulse delays. We explored whether some of the deviations can be explained by imperfection of the RF pulses due to B_1 inhomogeneity across the sample and inaccurate determination of flip angles. We did so by adding a single multiplicative tuning factor to the flip angles in the simulation. For all inter-pulse delays, the simulated spectra depended on the flip angle of the $\pi/2$ and π pulses. A full description of the simulation results with varying flip angles, along with estimation of the B_1^+ map of the coil used in the experiments is given in S1 in the supplementary material. Fig. 6 shows the effectiveness of the removal of the J-modulation on the echo train using the J-refocused CPMG sequence. Panels a, c and e show J-spectra of 2 M lactate in D_2O acquired with three inter-pulse delays using the standard CPMG sequence (blue) and the J-refocused CPMG sequence (brown). To test the efficacy of the decoupling effect of the J-refocused CPMG, the center peak was not removed in these spectra. It should be noted that in the J-refocused CPMG sequence, spectroscopic data are only acquired every other echo (see Fig. 3), thus the resulting bandwidth of the J-spectrum is $1/(4\tau)$, and not $1/(2\tau)$ as in the standard CPMG sequence. To match the bandwidth of both sequences, only even echoes from the non J-refocused CPMG data set were analyzed. The J-modulation is effectively removed from the J-spectra in all three conditions, although in some cases some modulation persists also in the J-refocused spectra. Panels b, d and f show difference spectra for three different inter-pulse delays, where in each the J-refocused spectrum was subtracted from the non J-refocused one. As expected from a decoupling scheme, the total spectral energy of the J-refocused spectra and the standard spectra should be preserved. This results in a stronger central line for the J-refocused spectra and a negative peak in the difference spectra. Away from the negative center peak, the difference spectra are dominated by the expected J modulation of the non-J-refocused CPMG data, as can be compared with those shown in Fig. 5.

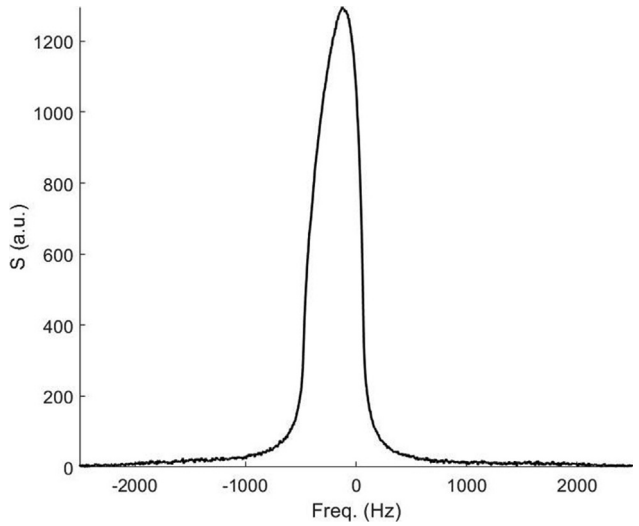

Fig. 4. 1D NMR spectrum of 2 M lactate in H_2O. No B_0 shimming was applied and the line width was about 500 Hz.

We tested the efficiency of the removal of the central peak with HSVD as a post-processing strategy for elimination of the contribution to the J-spectrum from water and other uncoupled protons when the water concentration is substantial. Fig. 7 shows data acquired from 2 M lactate solutions in H_2O and in D_2O. Here, three different values of CPMG inter-pulse delay were used. Panels on the left (a, c and e) show the spectra before the central peak removal for both phantoms, and those on the right (b,d and f) show the spectra after the center peak removal. Overall, the spectra obtained from both phantoms following the center peak removal are similar, both in terms of spectral content and SNR. Some addi-

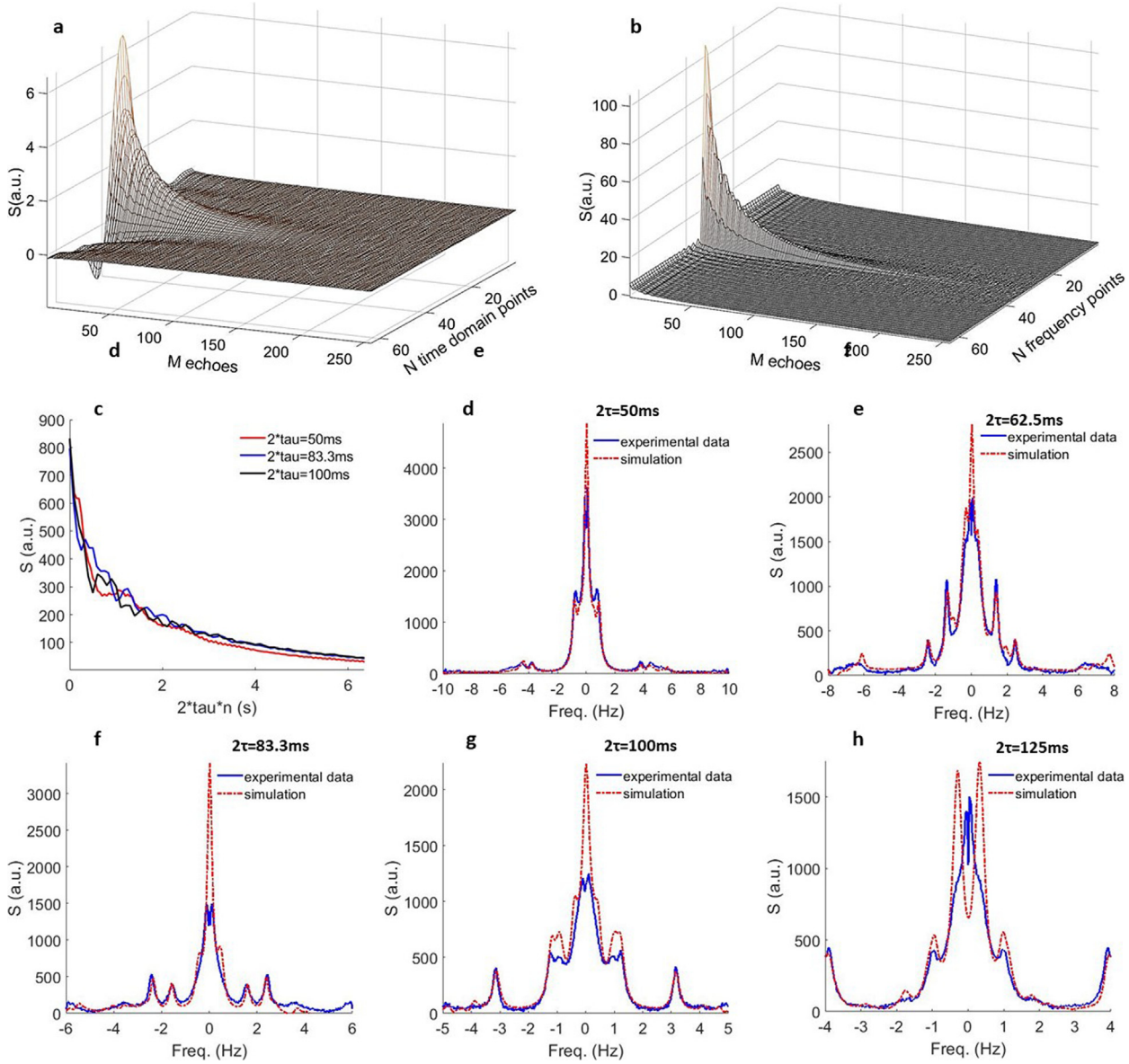

Fig. 5. (a) echo trains acquired with the spectroscopic CPMG sequence, with inter-pulse delay of 83.3 ms. (b) The data shown in (a) following echo symmetrisation and Fourier transformation along the acquisition time domain. The peak amplitude across echoes is used for time domain data shown in (c). (c) Time domain CPMG data obtained with three different inter-pulse delays. (d-h) J-spectra obtained from the Fourier transformation of such data as shown in (c) at 5 different inter-pulse delay values. Blue line: experimental results, red dashed-dotted line – simulation results. (For interpretation of the references to colour in this figure legend, the reader is referred to the web version of this article.)

tional small peaks are visible in the spectra obtained from the 2 M aqueous lactate solution. It is possible that these additional contributions to the spectra stem, for example from scalar coupling between the protonated hydroxyl group and the CH proton, but we have not explored this interpretation more rigorously at this time.

The second molecule which we chose to study is glutamate, which is a major metabolite in the ^{1}H NMR spectrum of the brain and is the main excitatory neurotransmitter. Protons in glutamate form a complex network of spin–spin coupling: glutamate protons remain strongly coupled even at high field, resulting in a non-trivial NMR spectrum of an AMNPQ system [36,37]. Panels a through c in Fig. 8 show the J-spectra obtained from a 2 M glutamate solution in D_2O at three different inter-pulse delays. There are no visible satellite peaks, and the residual effect of the J coupling is possibly exhibited in the line width. Also displayed on the same panels are simulations of the J-spectra of glutamate, performed with the same inter-pulse delays and windowed with a similar exponential filter as that used in the lactate simulations. These show indeed that no visible splitting is expected to be seen on the J-spectra under these conditions. In the supplementary figure S3 we show the three glutamate J-spectra with and without removal of the center peak, as well as the glutamate J-spectra obtained with the standard CPMG sequence and the J-refocused CPMG sequence, both indicating a negligible contribution of the J-coupling in glutamate to the J-spectra.

To estimate the SNR for the satellite peaks in the lactate spectrum in more realistic scenarios, we scanned a phantom containing a 100 mM solution of lactate in D_2O. This concentration was still about ten times higher than the expected concentration of lactate in disease (about 10 mM), but given the small phantom size and RF coil in our setup, it allowed the estimation of SNR in realistic

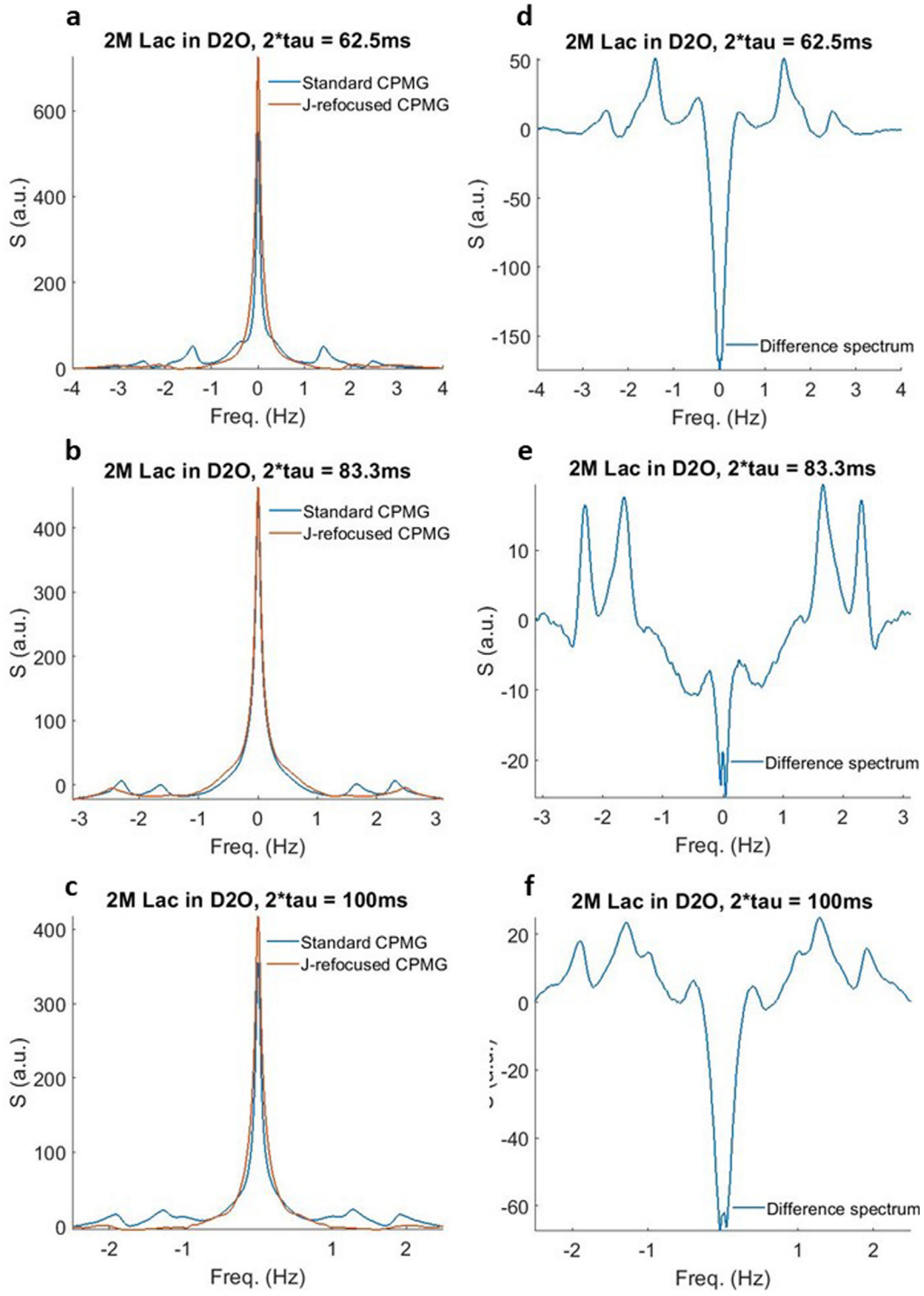

Fig. 6. (a–c) J-spectra of 2 M lactate in D_2O acquired with the standard CPMG sequence (blue) and the J-refocused CPMG sequence (brown). The decoupling effect of the J-refocused CPMG sequence is incomplete (see for example the peaks at ± 2.5 Hz in (b)), but the majority of the J-modulation is suppressed. (d-f) Difference spectra obtained by subtracting the J-refocused spectra from the standard ones. In all spectra the bandwidth is $1/(4\tau)$ and not $1/(2\tau)$, as data in the J-refocused CPMG are acquired every other echo. (For interpretation of the references to colour in this figure legend, the reader is referred to the web version of this article.)

conditions with reasonable scan times. The total scan time was about 10 min, and the number of averages was 32. J-spectra obtained from this phantom using three different inter-pulse delays are shown in Fig. 9. In this case, the time-domain data were multiplied by an exponential function emulating a T_2 of 2.45 s, matched to line width of the peaks at ± 3.1 Hz in the J-spectrum with inter-pulse delay of 100 ms, estimated at 0.13 Hz with the HSVD routine. The HSVD fit to each spectrum was subtracted from the experimental spectrum, and the residuals were used to calculate the standard deviation of the noise. The Cramér-Rao lower bounds (CRLB) are commonly used in NMR spectroscopy [38] and provide an alternative estimate of the SNR based on the HSVD

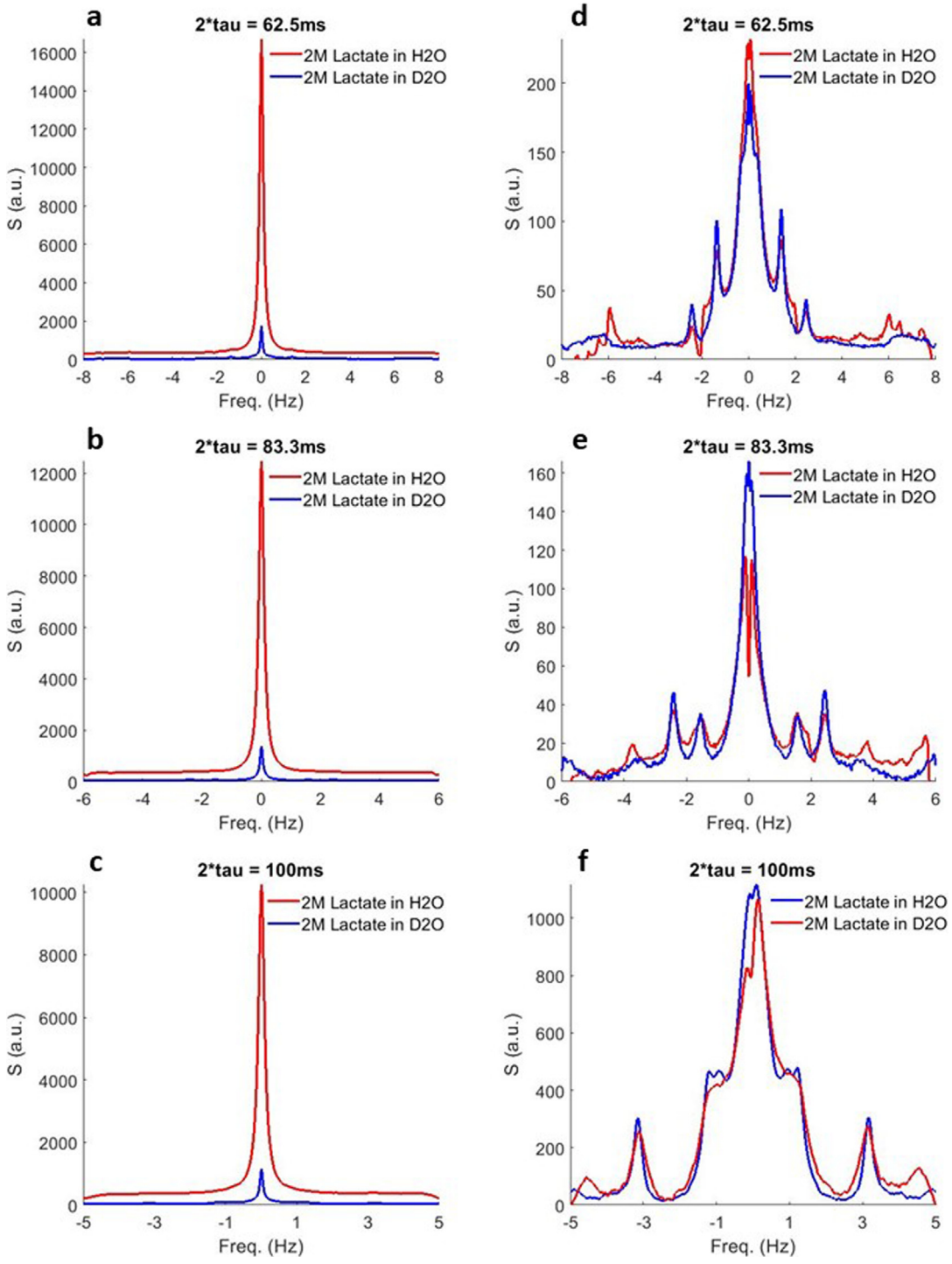

Fig. 7. (a–c) Spectra of 2 M lactate solutions in D_2O (blue) and in H_2O (red) before center peak removal for three different inter-pulse delays. (d–e) Same spectra after the removal of the center peak using HSVD. (For interpretation of the references to colour in this figure legend, the reader is referred to the web version of this article.)

fit and the noise properties of the unfiltered time domain data. The CRLB values for some of the resolved peaks in the J-spectra are given in Table 1, along with the estimates of the spectral parameters. The numbers of the peaks correspond to the numbers indicated in the spectra shown in Fig. 9.

4. Discussion

We have demonstrated the possibility of obtaining unique spectral information on brain metabolites at B_0 = 0.05 T. At this low static magnetic field, directly obtaining 1D spectra from the FID in a pulse-acquire experiment is all but impossible. J-spectroscopy, or the Fourier transform of the series of echoes acquired with a CPMG sequence, retains the information on spin–spin couplings, and well-resolved J-spectra of certain brain metabolites can be obtained. At a static field of 0.05 T, the spin systems comprising the protons in these metabolites all become strongly coupled, and the relations between the chemical shifts, scalar coupling constants and the π-π inter-pulse delays all contribute to the resulting pattern of the resulting J-spectrum for each

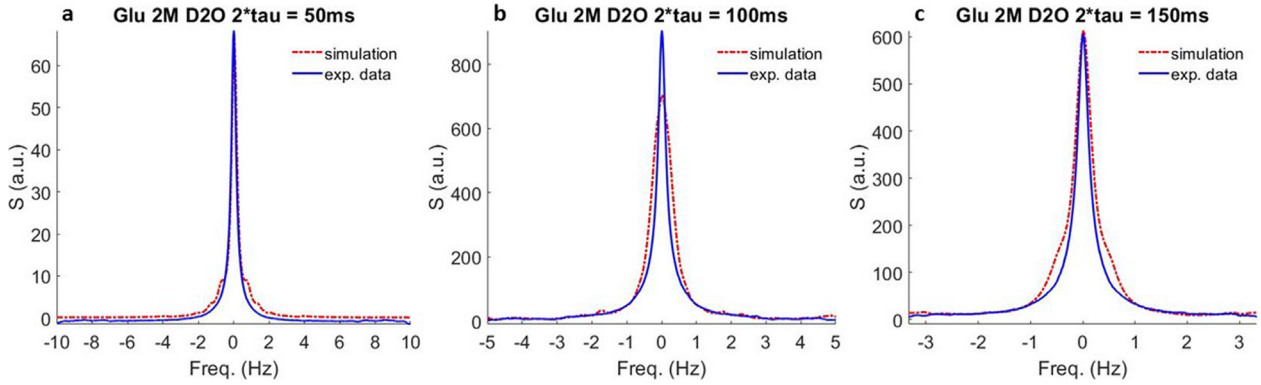

Fig. 8. Spectra obtained from a 2 M solution of glutamate in D_2O. (a–c) J-spectra of 2 M glutamate in D_2O acquired with three different inter-pulse delays of 50 ms, 100 ms and 150 ms (solid blue line), and simulations of these spectra for the same conditions (dashed-dotted red line). Neither the experimental spectra nor the simulations show visible satellite peaks. (For interpretation of the references to colour in this figure legend, the reader is referred to the web version of this article.)

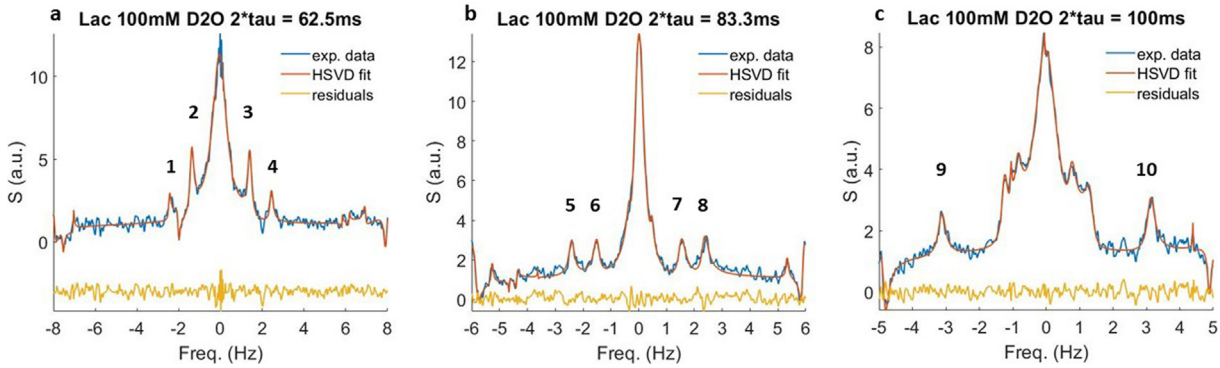

Fig. 9. J-spectra of 100 mM lactate in D_2O acquired at three inter-pulse delays: 62.5 ms (a), 83.3 ms (b) and 100 ms (c). Experimental data is shown in blue, HSVD fit in brown and residuals in yellow. Line broadening of 0.13 Hz was used. HSVD fitting results for the peaks marked with arrows is given in Table 1. (For interpretation of the references to colour in this figure legend, the reader is referred to the web version of this article.)

Table 1
HSVD analysis of J-spectra of 100 mM solutions of lactate in D_2O.

	Peak number on Fig. 9	Amplitude (a.u.)	Frequency (Hz)	Linewidth (Hz)	CRLB (% S.D)
τ = 62.5 ms	1	4.4	−2.45	0.13	22.4
	2	16.6	−1.40	0.23	6.8
	3	18.6	1.39	0.24	7.2
	4	5.7	2.41	0.18	15.4
2τ = 83.3 ms	5	10.8	−2.36	0.20	12.3
	6	12.7	−1.43	0.28	12.6
	7	12.4	1.43	0.25	12.1
	8	13.7	2.36	0.24	10.6
2τ = 100 ms	9	12.4	−3.12	0.27	13.9
	10	14.7	3.10	0.25	11.2

molecule. Some brain metabolites, such as creatine and phosphocreatine, are characterized by singlets alone, and therefore will only contribute to the zero-frequency line in a J-spectrum. The δ/J ratio of lactate at B_0 = 0.05 T, on the other hand, is large enough to yield well resolved J-spectra over a range of inter-pulse delay values. Other J-coupled metabolites, such as glutamate, contribute only to a broad component around the zero-frequency line, and cannot be resolved from one another. Of the six most prominent brain metabolites, only NAA and lactate result in well resolved peaks in the J-spectrum at B_0 = 0.05 T, and are well separated from one another. This give us hope that given enough SNR, it is possible to detect and quantify lactate in the brain in disease conditions, where lactate concentrations can increase from negligible levels to about 10 mM, a relatively high concentration compared to other prominent metabolites. The separability of peaks in the J-spectrum will depend on δ/J for each J-coupled metabolite, and thus on B_0. This means that it is possible that metabolites such as glutamate that do not produce a well-resolved J-spectrum at 0.05 T, will be detectable at higher B_0 still in the low-field regime. We will be investigate the range of possibilities in the future with additional simulations.

We focused in this work on showing the possibility of obtaining well-resolved J-spectra of lactate, an important metabolite in both brain and muscle, whose concentration in the brain increases in several diseases. The lactate spectra at B_0 = 0.05 T presents as that of an AB_3 system, and as was elegantly shown by Diehl et al.[15], this spectrum can be decomposed into two distinct sub-spectra, of which one is a well-characterized [I_A = ½ I_B = ½] AB spectrum. The time-dependent echo modulation of an AB system in a Carr-Purcell experiment was fully explored and given an analytical

expression by Wells and Gutowsky [17]. Interestingly, the prevalence of an AB sub-spectrum with [I_A = ½ I_B = ½] in the AB_3 spectrum is not limited only to the standard 1D spectrum, but can be seen also in J-spectrum of the AB_3 system. We provide evidence for this in part S4 in the supplementary material, where we show calculated J-spectra of an AB system obtained using the analytical expression given in Wells and Gutowsky, alongside simulations of AB_3 spectra with the same J and δ.

An important factor that will determine the possibility to detect and resolve J-spectra of metabolites at low field is the proton T_2 of these metabolites at such field strengths. The line width of peaks in the J-spectrum is given by $\Delta\upsilon_{1/2} = 1/(\pi T_2)$ and in our J-spectra of lactate this corresponded to a T_2 of about 3 s. This resulted in well-separated spectral contributions to the J-spectra at different inter-pulse delay values, barred the peaks close to the zero-frequency line. Metabolite relaxation times *in vivo* are expected to be shorter, and the resulting broader peaks potentially limit the separability of the contribution of lactate from that of NAA, and effectively reduce the SNR in the acquired spectra. There are no literature values for relaxation times of lactate and other metabolites *in vivo* at very low fields. Reported T_2 values of metabolites at 1.5 T are encouraging: 499 ms for NAA and 1022 ms for lactate [39]. For T_2 = 1022 ms, the resulting line width is of 0.3 Hz, well below the line width needed to separate the satellite peaks in the lactate J-spectrum from those of, e.g. NAA and the broad central line, dominated by the relatively short T_2 of water. Water T_2 values measured in *ex-vivo* tissue samples at low field (0.12 T) were about 115 ms [40,41], corresponding to a line width of 2.1 Hz. More recent results obtained from the human brain with an ultralow field MRI (ULFMRI) system operating at 130μT indicate a T_2 of 85 ms for brain tissue [42] It. The short T_2 of water compared to that of metabolites can also be used to significantly attenuate the water contribution to the J-spectrum by omitting some of the first echoes in the echo train, and thus obtaining a "T_2-weighted" J-spectrum. This will result in a first order phase variation in the J-spectrum that can be removed in the post-processing stage.

A significant challenge for J-spectroscopy is the removal of the peak around zero frequency, consisting of the contributions from water protons and all other singlets as well as from unresolved low frequency peaks in the J spectrum. One possible approach is to notch the peak in the post-processing stage, as we demonstrated here with the use of HSVD. In a standard time domain sampling scheme, the efficacy of this method is determined by how well the noise is sampled at the ADC level, and at three to four orders of magnitude between the water and metabolite signal the noise is typically undersampled, leading to loss of signal in the resulting spectrum. Reducing the noise power can be achieved by oversampling of the FID, as is done routinely in commercial MRI and NMR scanners operating at high field, allowing thus for acquisition of spectroscopic data without water suppression in various approaches [43–46]. The current configuration of our scanner is primarily aimed at generating MR images with cost-controlled components. In particular, the current 16-bit resolution of the analogue to digital converter (ADC) and a second-stage amplifier with limited gain preclude the proper sampling of the signal of low-concentration metabolites, and thus our current configuration is not ideally suited for detecting low concentration metabolites in fully realistic conditions. In this work we focused on demonstrating the feasibility of the general principle of notching the singlet signal in the J-spectrum, and further work will be invested in making it work in realistic conditions. Another approach we demonstrated here that can be used for the elimination of the singlet peak is by acquiring an additional J-spectrum in which the modulation induced by the scalar coupling is removed with the use of the J-refocused CPMG sequence. Subtraction of two spectra, one acquired with standard CPMG and the other with J-refocused CPMG results in a difference spectrum that contains only the contribution of J-coupled spins. This is a similar approach to spectral editing strategies commonly applied in *in vivo* NMR [47] albeit in this case it is not aimed at a specific metabolite but to J-coupled systems in general, in the way that broadband decoupling is performed. The decoupling efficacy of J-refocused spin echo sequences varies according to the spin system. Full decoupling is achievable only for a weakly coupled AX system, and in other spin systems decoupling is incomplete [29,31]. Indeed, the J-refocused CPMG results shown in Fig. 6 clearly indicate an incomplete refocusing of the J-coupling in lactate. In practice, though, the decoupling is efficient enough to generate a distinct difference spectrum that preserves the main features of the non-decoupled J-spectrum. Although attractive in some respects, this approach has a steep cost in SNR when compared to the alternative of subtracting the singlet peak, when similar acquisition times are considered, since two separate spectra have to be acquired, and the noise is additive in difference spectra.

Our goal is to provide the possibility of measuring metabolites, and in particular lactate, *in vivo*, especially in conditions where lactate increases globally in the brain, as is the case in neonatal hypoxic ischemia. While we have not provided data on J-spectra of metabolite solutions in concentrations expected in *in vivo* measurements, a rough estimate can be obtained from the data acquired from the 100 mM lactate solution. A rough estimation of the SNR based on the data acquired with 32 averages can be obtained from the isolated peaks in the spectrum in panel c of Fig. 9, acquired with inter-pulse delay of 100 ms. The SNR in this case is about 13, and corresponds to an acquisition time of 10 min. Our experiments were performed on a volume of 30 cc, whereas the total neonatal brain tissue is estimated on average at 360 cc [48]. Assuming a 15 cm diameter coil with similar characteristics to the 3.5 cm diameter coil we used [49], a lactate concentration of 10 mM in disease condition, and an inverse relationship between SNR and the radius of the solenoid coil, we expect SNR ≈ 5. It is worthwhile noting that while in standard MRS, the increase in SNR that accompanies increase in volume is mitigated by line broadening caused by decrease in B_0 homogeneity within the larger volume. This is not the case in J-spectroscopy, where the line width is dictated by T_2 and is independent of B_0 homogeneity. Admittedly, our SNR estimate does not take into consideration deleterious factors such as shorter T_2 of the lactate protons *in vivo* resulting in broader spectral lines, strong background signal contributed by water and lipids, subject motion and others. In addition, the SNR will also depend on the inter-pulse delay in a non-trivial manner: decreased inter-pulse delay will better sample the echo train and contribute to better SNR, while the concomitant decrease in J-modulation frequency will deleteriously bring the side peaks closer to the broad center peak, and tend to decrease the amplitude of the outer peaks, as was discussed earlier. More work needs to be done for a more realistic assessment, and we hope that with additional optimization of our RF chain and signal sampling strategy we will be able to present such data in the near future. The SNR that can be reached in our scanner can be improved with a receiver with a higher analogue-to-digital converter dynamic range, particularly useful when dealing with digitization noise in the presence of a large residual water peak. In the periphery of the brain, SNR could be increased approximately threefold by using an eight-element receiver array [2]. The design of multi-coil arrays for low field MR is challenging, and in this context we see the main benefit as a coarse approach for signal localization, rather than using the coil array for parallel receiving. Finally, the methodology we describe here is not limited to our 0.05 T scanner, and implementation on

other existing low field MRI scanners operating at higher B_0 will expectedly result in higher SNR.

In our work we have not implemented any spatial localization in the spectroscopic pulse sequence, neither by adding selectivity to the RF pulses nor by spatially encoding the signal with phase encoding, as was done for example in the work of Manassen et al [25]. Spatial selectivity is important in several aspects, from excluding non-wanted signal contributions from extraneous tissue, such as fatty tissue surrounding the brain, to increased specificity to local tissue damage in the case of focal disease such as stroke and tumors. Spatial localization with phase encoding in any number of directions is attractive for a variety of reasons, among which the flexibility to choose between (low) spatial resolution and reverting to a single region of interest by summation of the contribution from any number of voxels. We intend to add localization to the sequence in the near future.

Lastly, the ultimate goal is to apply the methodology we propose here *in vivo*, and thus potential of J-resolved MRS to quantify metabolites *in vivo* should be properly assessed in realistic conditions that reflect the complexity of acquiring data in the human brain and other anatomies. Several factors will contribute to the feasibility of achieving this goal, among which the ability to properly resolve the contribution of different metabolites to the J-spectrum, the possibility of suppressing the signal from water and lipids, and the SNR that can be obtained in reasonable scan times. These depend on multiple factors, such as the coil size, the target organ/tissue, the static magnetic field and the RF chain. We intend to explore the feasibility of obtaining *in vivo* J-spectra using our scanner, and we hope that similar efforts will be attempted by other groups on other low-field scanners.

5. Conclusions

We demonstrated here the possibility of obtaining well-resolved J-spectra of lactate on a low field scanner operating at B_0 = 0.05 T. It is hoped that future improvements in receive hardware and signal sampling technology will make it feasible to measure lactate and other J-coupled metabolites of interest in the human brain with low field MR scanners, adding a useful and diagnostically valuable aspect of MR to the growing list of biomedical applications of low field MR systems.

Declaration of Competing Interest

The authors declare that they have no known competing financial interests or personal relationships that could have appeared to influence the work reported in this paper.

Acknowledgements

We thank Dr. Pierre-Gilles Henry from the Center for Magnetic Resonance Research at the University of Minnesota for providing us with the simulation platform we used in this work. The work presented here was supported by the Simon Stevin Meester Prize awarded to A.G.W. (NWO grant #14997).

Appendix A. Supplementary material

Supplementary data to this article can be found online at https://doi.org/10.1016/j.jmr.2020.106834.

References

[1] Ren ZH, Obruchkov S, Lu DW, Dykstra R, Huang SY. A low-field portable magnetic resonance imaging system for head imaging. 2017 Progress in Electromagnetics Research Symposium - Fall (PIERS - FALL). 2017:3042-3044
[2] C.Z. Cooley, J.P. Stockmann, B.D. Armstrong, M. Sarracanie, M.H. Lev, M.S. Rosen, et al., Two-dimensional imaging in a lightweight portable mri scanner without gradient coils, Magnet Reson. Med. 73 (2015) 872–883.
[3] C.Z. Cooley, M.W. Haskell, S.F. Cauley, C. Sappo, C.D. Lapierre, C.G. Ha, et al., Design of sparse halbach magnet arrays for portable mri using a genetic algorithm, IEEE T Magn. 54 (2018).
[4] J. Obungoloch, J.R. Harper, S. Consevage, I.M. Savukov, T. Neuberger, S. Tadigadapa, et al., Design of a sustainable prepolarizing magnetic resonance imaging system for infant hydrocephalus, Magn. Reson. Mater. Phy. 31 (2018) 665–676.
[5] J.P. Marques, F.F.J. Simonis, A.G. Webb, Low-field mri: An mr physics perspective, J. Magn. Reson. Imaging. 49 (2019) 1528–1542.
[6] O'Reilly T, Teeuwisse WM, de Gans D, Koolstra K, Webb AG. In vivo three-dimensional brain and extremity mri at 50 mt using a permanent magnet halbach array. arXiv e-prints. 2020:arXiv:2005.02834
[7] Cooley CZ, McDaniel PC, Stockmann JP, Abitha Srinivas S, Cauley S, Sliwiak M, et al. A portable brain mri scanner for underserved settings and point-of-care imaging. arXiv e-prints. 2020:arXiv:2004.13183
[8] M. Sarracanie, C.D. LaPierre, N. Salameh, D.E.J. Waddington, T. Witzel, M.S. Rosen, Low-cost high-performance mri, Sci. Rep. 5 (2015) 15177.
[9] L.M. Broche, P.J. Ross, G.R. Davies, M.J. MacLeod, D.J. Lurie, A whole-body fast field-cycling scanner for clinical molecular imaging studies, Sci. Rep. 9 (2019) 10402.
[10] M.J. Macleod, L. Broche, J. Ross, G. Guzman-Guttierez, D. Lurie, A novel imaging modality (fast field-cycling mri) identifies ischaemic stroke at ultra-low magnetic field strength, Int J Stroke 13 (2018) 62–63.
[11] G. Oz, J.R. Alger, P.B. Barker, R. Bartha, A. Bizzi, C. Boesch, et al., Clinical proton mr spectroscopy in central nervous system disorders, Radiology 270 (2014) 658–679.
[12] L.A. Brandao, C. Caires, Hypoxic-ischemic injuries: The role of magnetic resonance spectroscopy, Neuroimaging Clin. N. Am. 23 (2013) 449–457.
[13] D. Xu, D. Vigneron, Magnetic resonance spectroscopy imaging of the newborn brain–a technical review, Semin. Perinatol. 34 (2010) 20–27.
[14] V. Govindaraju, K. Young, A.A. Maudsley, Proton nmr chemical shifts and coupling constants for brain metabolites, NMR Biomed. 13 (2000) 129–153.
[15] P. Diehl, R.G. Jones, H.J. Bernstein, A simplified procedure for analysis of complex nuclear magnetic resonance spectra.I. Principles of sub-spectral analysis, Can. J. Chem. 43 (1965) 81.
[16] R.K. Harris, Nuclear magnetic resonance spectroscopy, John Wiley & Sons, Inc, New York, 1986.
[17] E.J. Wells, H.S. Gutowsky, Nmr spin-echo trains for a coupled 2-spin system, J. Chem. Phys. 43 (1965) 3414–4000.
[18] R.L. Vold, R.R. Vold, Nuclear magnetic-relaxation in coupled spin systems, Prog. Nucl. Mag. Res. Sp. 12 (1978) 79–133.
[19] A. Allerhand, Analysis of carr—purcell spin-echo nmr experiments on multiple-spin systems. I. The effect of homonuclear coupling, J. Chem. Phys. 44 (1966) 1–9.
[20] S. Meiboom, D. Gill, Modified spin-echo method for measuring nuclear relaxation times, Rev. Sci. Instrum. 29 (1958) 688–691.
[21] W.P. Aue, J. Karhan, R.R. Ernst, Homonuclear broad-band decoupling and 2-dimensional j-resolved nmr-spectroscopy, J. Chem. Phys. 64 (1976) 4226–4227.
[22] K. Nagayama, K. Wuthrich, P. Bachmann, R.R. Ernst, 2-dimensional j-resolved h-1 nmr-spectroscopy for studies of biological macromolecules, Biochem. Bioph. Res. Co. 78 (1977) 99–105.
[23] A. Bax, A.F. Mehlkopf, J. Smidt, A fast method for obtaining 2d j-resolved absorption-spectra, J. Magn. Reson. 40 (1980) 213–219.
[24] Y. Ke, B.M. Cohen, J.Y. Bang, M. Yang, P.F. Renshaw, Assessment of gaba concentration in human brain using two-dimensional proton magnetic resonance spectroscopy, Psychiatry Res. 100 (2000) 169–178.
[25] Y. Manassen, G. Navon, Spatially encoded spin echoes, j-imaging, J. Magn. Reson. 66 (1986) 568–572.
[26] H.S. Gutowsky, R.L. Vold, E.J. Wells, Theory of chemical exchange effects in magnetic resonance, J. Chem. Phys. 43 (1965) 4107–5000.
[27] T. O'Reilly, W.M. Teeuwisse, A.G. Webb, Three-dimensional mri in a homogenous 27cm diameter bore halbach array magnet, J. Magn. Reson. 307 (2019) 106578.
[28] B. de Vos, P. Fuchs, T. O'Reilly, A. Webb, R. Remis, Gradient coil design and realization for a halbach-based mri system, IEEE T Magn. 56 (2020).
[29] J.A. Aguilar, M. Nilsson, G. Bodenhausen, G.A. Morris, Spin echo nmr spectra without j modulation, Chem. Commun. (Camb.) 48 (2012) 811–813.
[30] K. Takegoshi, K. Ogura, K. Hikichi, A perfect spin-echo in a weakly homonuclear j-coupled 2 spin-1/2 system, J. Magn. Reson. 84 (1989) 611–615.
[31] P.C.M. Vanzijl, C.T.W. Moonen, M. Vonkienlin, Homonuclear-j refocusing in echo spectroscopy, J. Magn. Reson. 89 (1990) 28–40.
[32] L. Vanhamme, R.D. Fierro, S. Van Huffel, R. de Beer, Fast removal of residual water in proton spectra, J. Magn. Reson. 132 (1998) 197–203.
[33] R.V. Mulkern, J.L. Bowers, Calculating spectral modulations of ab-systems during press acquisitions, Magnet Reson. Med. 30 (1993) 518–519.
[34] R. Mulkern, J. Bowers, Density matrix calculations of ab spectra from multipulse sequences: Quantum mechanics meets in vivo spectroscopy, Concepts Magnetic Resonance 6 (1994) 1–23.
[35] P.G. Henry, M. Marjanska, J.D. Walls, J. Valette, R. Gruetter, K. Ugurbil, Proton-observed carbon-edited nmr spectroscopy in strongly coupled second-order spin systems, Magn. Reson. Med. 55 (2006) 250–257.

[36] V. Govindaraju, V.J. Basus, G.B. Matson, A.A. Maudsley, Measurement of chemical shifts and coupling constants for glutamate and glutamine, Magn. Reson. Med. 39 (1998) 1011–1013.
[37] R.B. Thompson, P.S. Allen, A new multiple quantum filter design procedure for use on strongly coupled spin systems found in vivo: Its application to glutamate, Magn. Reson. Med. 39 (1998) 762–771.
[38] S. Cavassila, S. Deval, C. Huegen, D. van Ormondt, D. Graveron-Demilly, Cramer-rao bound expressions for parametric estimation of overlapping peaks: Influence of prior knowledge, J. Magn. Reson. 143 (2000) 311–320.
[39] H. Kugel, B. Roth, F. Pillekamp, K. Kruger, O. Schulte, A. von Gontard, et al., Proton spectroscopic metabolite signal relaxation times in preterm infants: A prerequisite for quantitative spectroscopy in infant brain, J. Magn. Reson. Imaging 17 (2003) 634–640.
[40] P.A. Bottomley, T.H. Foster, R.E. Argersinger, L.M. Pfeifer, A review of normal tissue hydrogen nmr relaxation times and relaxation mechanisms from 1–100 mhz: Dependence on tissue type, nmr frequency, temperature, species, excision, and age, Med. Phys. 11 (1984) 425–448.
[41] G.L. Wolf, B. Conard, Nmr proton t1 and t2 relaxation times from fresh, in vitro canine tissues at 5.1 mhz, Physiol. Chem. Phys. Med. NMR 15 (1983) 19–22.
[42] B. Inglis, K. Buckenmaier, P. Sangiorgio, A.F. Pedersen, M.A. Nichols, J. Clarke, Mri of the human brain at 130 microtesla, Proc. Natl. Acad. Sci. U S A. 110 (2013) 19194–19201.
[43] Z. Dong, W. Dreher, D. Leibfritz, Toward quantitative short-echo-time in vivo proton mr spectroscopy without water suppression, Magn. Reson. Med. 55 (2006) 1441–1446.
[44] R.E. Hurd, D. Gurr, N. Sailasuta, Proton spectroscopy without water suppression: The oversampled j-resolved experiment, Magn. Reson. Med. 40 (1998) 343–347.
[45] J.M. Lin, S.Y. Tsai, H.S. Liu, H.W. Chung, R.V. Mulkern, C.M. Cheng, et al., Quantification of non-water-suppressed mr spectra with correction for motion-induced signal reduction, Magn. Reson. Med. 62 (2009) 1394–1403.
[46] H. Serrai, D.B. Clayton, L. Senhadji, C. Zuo, R.E. Lenkinski, Localized proton spectroscopy without water suppression: Removal of gradient induced frequency modulations by modulus signal selection, J. Magn. Reson. 154 (2002) 53–59.
[47] W. Bogner, G. Hangel, M. Esmaeili, O.C. Andronesi, 1d-spectral editing and 2d multispectral in vivo(1)h-mrs and (1)h-mrsi - methods and applications, Anal. Biochem. 529 (2017) 48–64.
[48] S. Wang, P. Fan, D. Xiong, P. Yang, J. Zheng, D. Zhao, Assessment of neonatal brain volume and growth at different postmenstrual ages by conventional mri, Medicine (Baltimore). 97 (2018) e11633.
[49] D.I. Hoult, P.C. Lauterbur, Sensitivity of the zeugmatographic experiment involving human samples, J. Magn. Reson. 34 (1979) 425–433.